ACS APPLIED POLYMER MATERIALS

pubs.acs.org/acsapm Article

Mesomorphic Intermediate Stages During Brill Transition of Nylon 6/6

Cheng-Yo Ho, Po-Hsun Chen,* Ching-Feng Yang, U-Ser Jeng, and An-Chung Su*

Cite This: *ACS Appl. Polym. Mater.* 2021, 3, 1042−1051 Read Online

ACCESS | Metrics & More | Article Recommendations | Supporting Information

ABSTRACT: The Brill transition in nylon 6/6 is generally perceived as a fully reversible solid−solid transformation between a low-temperature triclinic lattice (α-phase) and a high-temperature pseudohexagonal lattice; however, there is a *ca.* 7% density mismatch between these two structures, and so one would not expect a complete solid−solid transformation. The kinetic aspects of the Brill transition in nylon 6/6 during (1) cooling from the dominantly pseudohexagonal state and (2) heating of glassy specimen quenched from the molten state were analyzed *via in situ* small-/wide-angle X-ray scattering (SAXS/WAXS), Fourier-transform infrared spectroscopy (FTIR), and differential scanning calorimetry (DSC). For successfully deconvoluted WAXS profiles upon cooling, two additional reflections located between $(100)_\alpha$ and $(010/110)_\alpha$ positions are necessary when the temperature is below 200 °C. The FTIR spectra signify the incipient formation of α-crystals at 150 °C, and the SAXS invariant progressively increases from 150 to 110 °C instead of a sigmoidal jump, which indicates a gradual formation process of a high-density α-phase. Thus, the precursory split of the characteristic peak of a high-temperature phase in WAXS profiles can only be attributed to an intermediate form of mesomorphic nature. Upon heating the quenched glassy specimen, the mesomorphic phase content increases at the full expense of the α-phase (with additional contribution from the amorphous phase), followed by the plateaued mesomorphic phase content, which then transformed into pseudohexagonal structures at 180 °C. The 2D correlation maps of N−H stretching bands also give consistent results, which indicate that the mesomorphic phase is generated from both the amorphous phase and α-crystals. Both cooling and heating processes indicate the existence of a mesomorphic intermediate between high-temperature pseudohexagonal and low-temperature triclinic (α) phases; hence, the Brill transition in nylon 6/6 is not a direct solid-to-solid transformation, but a continuous melting−recrystallization process. This bears significance in addressing mechanical properties of nylons in the vicinity of Brill transition temperature.

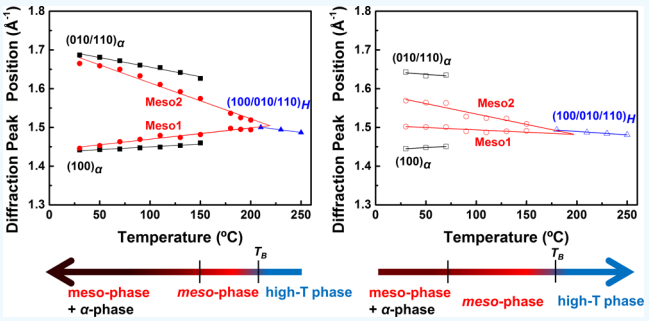

KEYWORDS: *aliphatic polyamide 6/6, Brill transition, phase transition, small-/wide-angle X-ray scattering (SAXS/WAXS), fourier-transform infrared spectroscopy (FTIR), differential scanning calorimetry (DSC)*

Downloaded via NATL TSING HUA UNIV on April 6, 2021 at 02:05:34 (UTC).
See https://pubs.acs.org/sharingguidelines for options on how to legitimately share published articles.

INTRODUCTION

Nylons, or aliphatic polyamides, are semicrystalline polymers that offer enhanced mechanical properties, good chemical resistance, and various thermal properties; therefore, nylons are widely used in various fields such as fibers, textiles, automotive, and electrical/electronic parts.[1] In view of the widespread application of nylons, precise control of the crystalline order, which is closely related to the mechanical properties, is of substantial importance. At the high-temperature end, the Brill transition (first reported by Brill[2] in 1942 for nylon 6/6) demonstrates an apparently reversible solid−solid transition between the room-temperature triclinic structure (α-phase) and the elevated-temperature pseudohexagonal structure. This phase transformation can be obviously observed *via* X-ray diffraction (XRD), which shows that the well-separated $(100)_\alpha$ and $(010/110)_\alpha$ reflection peaks gradually merge into a fully overlapped single reflection peak of $(100/010/110)_H$ upon heating and the pseudohexagonal structure reverts to the higher density triclinic structure upon cooling.[3−7] The temperature that these two reflections merge completely at is defined as "Brill transition temperature (T_B)," and T_B is not fixed at a specific temperature but depends on the crystallization condition.[4,5] Brill proposed that this transformation between the triclinic and pseudohexagonal phases results from the generation of the three-dimensional hydrogen bond cross-linking network, implying a direct solid−solid transition.[2] Later studies indicated that the suggested three-

Received: November 23, 2020
Accepted: December 18, 2020
Published: January 4, 2021

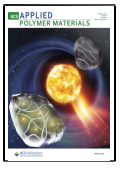

© 2021 American Chemical Society

https://dx.doi.org/10.1021/acsapm.0c01303
ACS Appl. Polym. Mater. 2021, 3, 1042−1051

dimensional hydrogen-bond network does not exist and the hydrogen bonds that formed at room temperature stay intact until melting.[3,8−16] Another model has been proposed that the pseudohexagonal structure at elevated temperatures is actually a triclinic structure with the hydrogen bonds arranged in sheets, and the projection along the *c*-axis has the hexagonal symmetry.[3]

Although the Brill transition can be clearly monitored *via* XRD, its nature is controversial. In calorimetry studies, a sharp endothermic peak at T_B can barely be observed except for the solution-crystallized case.[4,5,14] T_B in nylon 6/6 shows a hysteresis effect, where T_B on the heating process is higher than that on the cooling process, suggesting a first-order transition.[4] In contrast, Xenopoulos and Wunderlich pointed out that the Brill transition is not a first-order transition, as conformational disorder is gradually introduced into the nylon 6/6 crystals upon heating, with concurrent packing density changes during transformation.[5] It is then suggested that the Brill transition may inherently be a first-order process but comprises a second-order element.[6] Variable-temperature XRD and nuclear magnetic spectroscopy measurements showed that the low- and high-melting phases of nylon 6/6 coexist in a fairly broad temperature range and the triclinic-to-pseudohexagonal transition appears gradual rather than abrupt.[10] Infrared spectroscopy techniques, such as polarized FITR,[11,13,17−20] 2D correlation infrared spectroscopy,[21] and Raman spectroscopy,[15,22] were also used to investigate the transition mechanism at the functional group level, supporting the concept that the Brill transition is a gradual process, with the chain conformation changing within a temperature range rather than across a specific temperature. Results of these studies on the Brill transition in nylon 6/6 cast doubts on the original assignment of a straightforward solid−solid transformation.

Apart from the nylon 6/6 system, the Brill transition has also been widely discussed in numerous nylons such as nylon 6,[13,23−26] nylon 11,[23,27] and other even−even or odd−even nylons.[8,17,26,28−41] Nevertheless, not all the cases showed the typically reversible Brill transition while using the emerging/splitting of reflection peaks as a criterion upon heating and cooling. For instance, results of nylon 10/10 revealed that no Brill transition occurs for the melt-crystallized sample, but the transition can be identified for the cold-crystallized sample based on the criterion of merging reflections. However, subsequent cooling of the cold-crystallization sample shows a direct split of the γ-phase reflection peak instead of a reversible phenomenon, undermining again the attribution to a solid−solid transition.[38] For nylon 5/6, WAXS and SAXS evidences[36] demonstrated Brill-like transition upon heating, but without backward transition during subsequent cooling.

In particular, nylon 6 is known to display two monoclinic crystalline structures, namely, α- and γ-phase and one pseudohexagonal "mesomorphic" β-phase, which is obtained by quenching from the molten state and appears partially disordered from the XRD pattern.[23,25,42,43] Auriemma et al.[25] pointed out that the β-phase of nylon 6 comprises small mesomorphic aggregates of conformationally disordered but straight chains arranged in a hexagonal lattice; the hydrogen bonds within the β-phase formed nearly completely but without specific crystallographic direction; besides, the disorder is related to the history of the sample. Mileva et al.[43] reported that both in the melt-crystallization process (from the equilibrium melt) and in the cold-crystallization process (from the as-quenched glass), the mesomorphic phase formed near glass transition temperature (T_g), that is, high supercooling in melt-crystallization and slow heating in cold-crystallization. Thus, the mesomorphic phase (or "mesophase") is not a perfect structure and usually appears as an intermediate or precursor en route to a more stable structure. As proposed by Strobl,[44] the mesomorphic domains are formed first in the induction period of the crystallization process; these mesomorphic domains transform into a granular crystalline phase before finally coalescing into lamellar crystals. In our previous study of the racemic polylactide blend upon slow cooling from the molten state, FTIR results indicated the development of the racemic ($3_2/3_1$) helical pairs and a broad mesomorphic peak emerging in the WAXS profile before the appearance of stereocomplex (β_c) crystals, indicating that the formation of β_c crystals is *via* an intermediate stage of clustered helical pairs as the mesomorphic phase.[45] The gradual development of the primary nucleation process is also supported by a molecular dynamics study of polyethylene in a semidilute solution.[46]

By definition, solid−solid transition is a direct transformation that occurs in the solid state from one crystalline form to another without entering an isotropic liquid phase; thus, the positional changes of the molecules before and after the transition must not be too large such that long-range diffusion is not involved.[47] For poly(9,9-di-*n*-hexyl-2,7-fluorene),[48] the direct transformation from the high-temperature monoclinic α-phase to the low-temperature triclinic α'-phase upon step-wise cooling has been reported; the conversion of this α-to-α' solid−solid transition is limited because of the density mismatch of *ca.* 1.5%, as demonstrated by extensively observed transformation-induced cracking. In the case of poly(butylene adipate),[49] it has been observed that kinetically preferred orthorhombic β-crystals transform directly into the thermodynamically favored monoclinic α-crystals upon annealing at a sufficiently high temperature, with *ca.* 1.8% density difference between the two crystalline phases. It is then interesting to note that the density difference between the high-temperature pseudohexagonal structure and low-temperature triclinic structure in nylon 6/6 is *ca.* 7% (*cf.* Supporting Information, density changes due to thermal expansion) in the reported transformation temperature range of 150−210 °C, which is significantly higher than those in the two examples of solid−solid transition. It is thus of interest to take a better look over the mechanistic route of Brill transition. With finely deconvoluted WAXS profiles and the support of IR spectra, here we show that the structural evolution during the Brill transition between high-temperature pseudohexagonal and the low-temperature triclinic (α) phases is a gradual melting−recrystallization process and not a direct solid−solid transformation.

EXPERIMENTAL DETAILS

Sample. The nylon 6/6 sample (Zytel 42 nylon resin) with a weight−average molecular weight M_w = 233 kDa and a polydispersity index PDI = 1.9 was purchased from Sigma-Aldrich and used as received.

Instrumental Setup. Simultaneously, *in situ* small-/wide-angle X-ray scattering (SAXS/WAXS) measurements were carried out at the Taiwan Light Source (TLS) beamline BL23A, National Synchrotron Radiation Research Center (NSRRC), providing a high flux beam of 10^{11} photons/s for scattering time resolution within a second and covering the energy range between 5 and 23 keV.[50] The nylon 6/6 was sealed into the punctured Al pans (*ca.* 0.7 mm in thickness and 6 mm in diameter) with Kapton windows for the X-ray incident beam,

https://dx.doi.org/10.1021/acsapm.0c01303
ACS Appl. Polym. Mater. 2021, 3, 1042−1051

and the INSTEC HCS302 sample holder was used as the temperature controller. With 10 keV beam (wavelength λ = 1.24 Å), the *in situ* SAXS and WAXS profiles were collected using a Pilatus 1M-F area detector (169 × 179 mm^2) and a three-series Mythen-1K linear detector (8 × 18 mm^2) with 10 °C/min rate, respectively. The instrumental setup covered the SAXS q-range of 0.005−0.367 Å^{-1} and WAXS q-range of 0.78−2 Å^{-1}. The scattering wave vector $q = 4\pi\lambda^{-1}\sin\theta$ (with 2θ being the scattering angle) was calibrated by using silver behenate for SAXS and polyethylene for WAXS. Fluorescence spectra from an iron sheet were used to calibrate the pixel sensitivity of the SAXS and WAXS detectors; all SAXS and WAXS data were corrected with sample transmission, background scattering, and detector noise. The SAXS data were placed in the absolute intensity scale by the use of a precalibrated high-density polyethylene standard.

Differential scanning calorimetry (DSC) measurements were conducted by using the PerkinElmer Diamond instrument with purging nitrogen gas (20 mL/min) at a heating/cooling rate of 10 °C/min between 30 and 280 °C. For Fourier-transform infrared spectroscopy (FTIR), nylon 6/6 pellets were dissolved in formic acid and cast on the KBr plate to form a thin film and the spectra were recorded by using the PerkinElmer Spectrum RXI spectrophotometer at a resolution of 1 cm^{-1} and averaged over 32 scans. During the collection, the specimen was put into the INSTEC HCS402 sample holder and the temperature was controlled by INSTEC mk1000 with a 10 °C/min rate.

Data Analysis. The SAXS profiles can be modeled by $I(q) = I_0P(q)S(q)$,[51] where $P(q)$ is the normalized form factor [*i.e.*, $P(0) = 1$], which represents the shape of the nanodomains, and $S(q)$ is the structure factor, which stands for spatial correlation among the scattering nanoparticles. Zero-angle scattering (I_0) is correlated to particle numbers (n_p), particle volume (V_p), and electron density contrast ($\Delta\rho$) [$I_0 = n_p(\Delta\rho)^2(V_p)^2$]. The scattering invariant Q_{inv} can be written as $Q = \int_0^\infty I(q)q^2dq$, representing the overall scattering power of the system and reflecting the heterogeneity in two-phase systems.[52,53] The relative scattering invariant will be integral from low-q to high-q limits of the SAXS profiles;[52] such approximation is appropriate, while the experimental q-range covers main changes.

The WAXS profiles were deconvoluted into combinations of Lorentz functions by using the PeakFit software. The phase composition is operationally defined as the peak area of the specific reflection over the total area under the experimental WAXS profile, and the d-spacings were obtained from the peak positions *via* the relation $d = 2\pi/q$.

The 2D correlation spectrum is a quantitative measure along the external variable t observed at two different spectral variables, ν_1 and ν_2, over some finite interval between T_{min} and T_{max}. The application in infrared spectra was first introduced by Noda.[54,55] The 2D correlation spectrum can be defined as $X(\nu_1, \nu_2) = \langle y(\nu_1, t)\cdot y(\nu_2, t')\rangle$, which can be further simplified as a complex number function $X(\nu_1, \nu_2) = \phi(\nu_1, \nu_2) + i\Psi(\nu_1, \nu_2)$. The synchronous 2D correlation intensity $\phi(\nu_1, \nu_2)$ represents the overall similarity or coincidental trends between different spectral variables within scanning t from T_{min} to T_{max}; the asynchronous 2D correlation intensity $\Psi(\nu_1, \nu_2)$, on the other hand, describes the sequential but not coincidental changes of spectral variables (out-of-phase character).[21,56] With the software 2DShige, composed by Shigeaki Morita, 2D correlation maps were generated. The positive synchronous cross-peak $\phi(\nu_1, \nu_2)$ sign stands for the intensity at ν_1 and ν_2 that synchronously increase or decrease within the observation interval; nevertheless, the negative synchronous cross-peak $\phi(\nu_1, \nu_2)$ sign indicates that one of the spectral intensities at ν_1 and ν_2 increases, whereas its counterpart decreases. As the case in the synchronous spectrum, the sign of an asynchronous cross-peak can be either positive or negative. If the intensity changes at ν_1 occur predominantly before those at ν_2, the sign of an asynchronous cross-peak $\Psi(\nu_1, \nu_2)$ becomes positive; otherwise, the peak sign becomes negative. The rule is reversed if the synchronous peaks become negative.

RESULTS AND DISCUSSION

Figure 1 shows the WAXS cooling profiles of nylon 6/6 from 250 to 30 °C at a 10 °C min^{-1} rate, showing a typical Brill transition process of pseudohexagonal-to-triclinic structure transformation upon cooling. At 250 °C, the profile gave only one reflection peak at q = 1.48 Å^{-1} (d-spacing: 4.24 Å), which is characterized as the $(100/010/110)_H$ reflection of the high-temperature pseudohexagonal structure (*i.e.*, "Brill structure"); upon cooling, the single reflection peak gradually splits into two peaks, shifting to lower and higher q-positions, respectively. The peak split occurred at *ca.* 210 °C; hence, 210 °C is considered to be the Brill transition temperature (T_B) upon cooling. After reaching 30 °C, the WAXS profiles gave a typical α-phase profile with $(100)_\alpha$ and $(010/110)_\alpha$ reflections located at q = 1.44 and 1.69 Å^{-1}, corresponding to the interchain distance of 4.36 Å within the hydrogen-bonded chains and the intersheet spacing of 3.72 Å within the hydrogen-bonded sheets, respectively.[4,6,7,30] According to the WAXS profiles, the intersheet spacing is more sensitive to temperature.

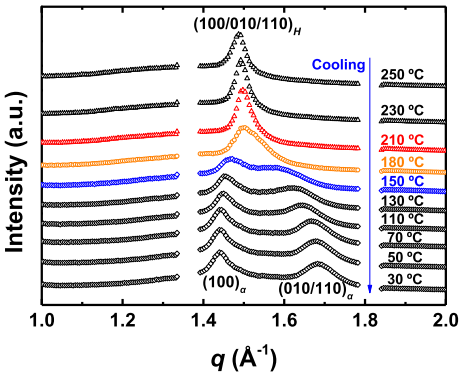

Figure 1. WAXS cooling profiles of nylon 6/6 from 250 to 30 °C at a 10 °C min^{-1} rate, giving a typical Brill transition process that the single reflection peak (pseudohexagonal structure) at an elevated temperature splits into two reflection peaks (triclinic structure) upon cooling. The split effect occurs at *ca.* 210 °C, which is defined as the Brill transition temperature (T_B).

In order to understand the structural evolution upon cooling, the WAXS profiles (*cf.* Figure 1) were deconvoluted under two common circumstances, as described in the Introduction section: (a) solid−solid transformation during the Brill transition and (b) the high-temperature structure and low-temperature α-phase coexist in the specific temperature range. First, the direct pseudohexagonal-to-triclinic solid−solid transformation at the Brill transition temperature was assumed, and the representative deconvoluted profile is shown in Figure S2a. According to this assumption, the phase development upon cooling is illustrated in Figure 2a. The population of the high-temperature pseudohexagonal structure increases with the decreasing temperature; after being transformed to the α-phase, the α-phase population increases rapidly up to *ca.* 65% at 130 °C and then decreases drastically to *ca.* 25% at 110 °C, followed by a progressive increase to *ca.* 35% during further cooling. This anomalous decrease of α-phase population between 130 and 110 °C contradicts the concept that the α-phase is the room-temperature stable structure. Thus, the solid−solid transition cannot describe the Brill transition satisfactorily. Then, the coexistence of high- and low-temperature structures is assumed for deconvolution of the

https://dx.doi.org/10.1021/acsapm.0c01303
ACS Appl. Polym. Mater. 2021, 3, 1042−1051

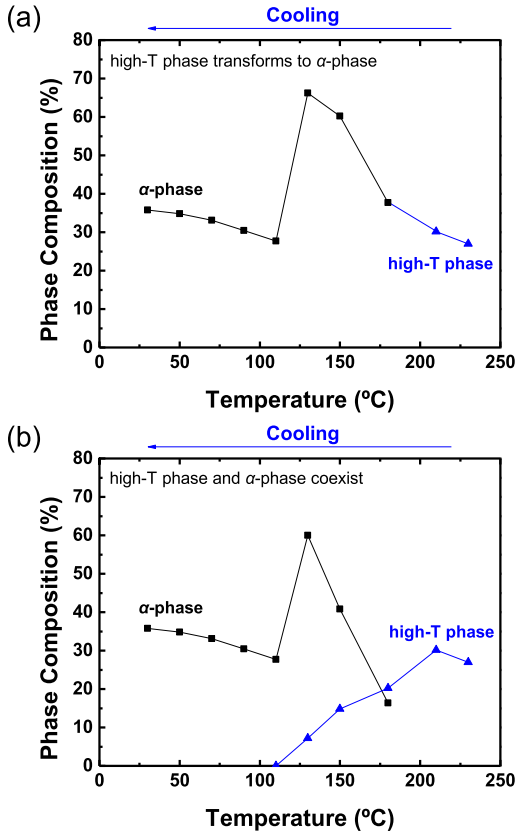

Figure 2. Evolution of phase composition upon cooling with (a) pseudohexagonal-to-triclinic solid−solid transition model and (b) pseudohexagonal- and triclinic-structure coexistence (in the 180−130 °C temperature range) model. In both cases, all the populations of α-phase show an abrupt decrease from 130 to 110 °C, which contradicts the concept that the α-phase is a room temperature-stable structure.

WAXS profile, and the representative deconvoluted profile is shown in Figure S2b. Figure 2b shows the phase evolution for the coexistence model. Upon cooling, the population of the pseudohexagonal structure gradually decreases, whereas the population of the α-phase increases; however, this coexistence model also gives a peculiar decrease of the α-phase population after 130 °C. The results of these two transformed models denote that neither the solid−solid transition nor the coexistence of pseudohexagonal- and triclinic-structures can adequately describe the Brill transition.

In order to have more reasonable results, another two reflection peaks in the middle q-region between $(100)_\alpha$ and $(010/110)_\alpha$ reflections are added below T_B, and the representative deconvoluted profile is illustrated in Figure S2c. After introducing these two additional reflections, which represent the intermediate mesomorphic phase, the corresponding phase composition and the DSC trace upon cooling are shown in Figure 3a. From 250 to 210 °C, the fraction of the high-temperature phase (ϕ_H) increases, while the fraction of the amorphous phase ($\phi_{amorphous}$) decreases, which is accompanied by an exothermal behavior, suggesting that the pseudohexagonal structure is generated from the amorphous phase. When the temperature is below 210 °C, a broad exothermal peak can be observed in the DSC trace, and the high-temperature phase transforms into the mesomorphic phase. The fraction of the mesomorphic phase (ϕ_{meso}) continuously increases upon cooling with the decreasing

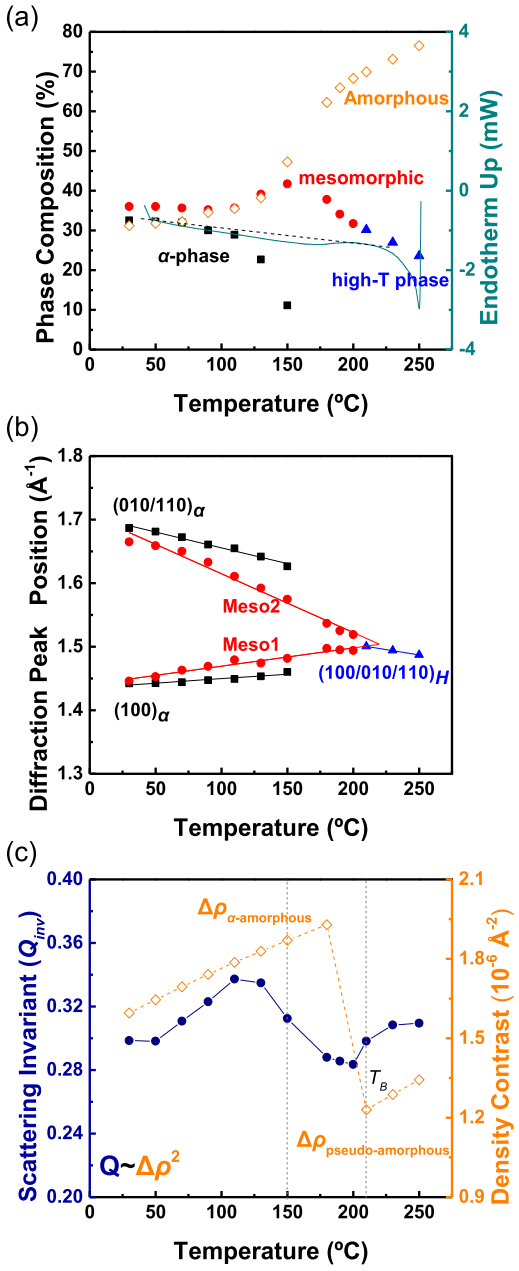

Figure 3. (a) Evolution of phase composition upon cooling (symbols, including the pseudohexagonal high-temperature phase, triclinic α-phase, amorphous phase, and mesomorphic phase) and the corresponding DSC thermal trace (line). (b) Development of the peak positions upon cooling, indicating that T_B is at *ca.* 210 °C, and the α-phase emerge below 150 °C. The solid lines represent the linear-fit of d-spacing for each phase. (c) Scattering invariant (Q_{inv}, blue line) calculated from the experimental SAXS profile and the theoretical density contrast (orange line) of the solid−solid transition. (*cf.* Figure S4 and density changes due to thermal expansion in Supporting Information).

$\phi_{amorphous}$, while ϕ_{meso} reaches its maximum at 150 °C. With subsequent cooling from 150 to 110 °C, the α-phase (ϕ_α) emerges and the population increases to *ca.* 20%, which is contributed by both the mesomorphic and the amorphous (majority) phases, implying that the α-phase can be generated from the amorphous phase and the transformation route from the pseudohexagonal phase to the mesomorphic phase and then to the α-phase. Below 110 °C, ϕ_α slightly increases to *ca.*

https://dx.doi.org/10.1021/acsapm.0c01303
ACS Appl. Polym. Mater. 2021, 3, 1042−1051

30%, which is almost contributed entirely by the decrease of $\phi_{amorphous}$. Depending on the evolution of phase composition, the broad exothermal peak below 210 °C indicates the formation of mesomorphic and α-phases.

Figure 3b gives the development of the reflection peak position upon cooling according to the mesomorphic model. Between 250 and 210 °C, the WAXS profile gave only a single reflection peak of the high-temperature pseudohexagonal structure, and this single reflection peak splits into two peaks below 210 °C, with the apparent change in the linear thermal expansion coefficient (α_T) calculated by the linear fit of d-spacing, as represented by solid lines, which indicates that α_T $(H) = 3.35 \times 10^{-4}$ to α_T $(m_1) = -2.88 \times 10^{-4}$ and α_T $(m_2) = 9.25 \times 10^{-4}$. The anomalous temperature dependence of the two WAXS peaks of the mesomorphic phase (red solid lines) implies that the peak split at *ca.* 210 °C does not stand for the thermal expansion of the high-temperature phase. Besides, another two reflection peaks that should be classified into the α-phase emerge after 150 °C. Thus, the peak split along the different thermal expansion coefficients below 210 °C represents a transition from the high-temperature phase to the mesomorphic phase.

The concept of phase transition *via* a mesomorphic intermediate can be supported by the SAXS profiles, which represent the scattering ability of the nanograins. Because of the 8% density difference between pseudohexagonal and triclinic lattices, the scattering length density (SLD) of the α-phase is greater than that of the high-temperature phase, and the SLD contrast between α and amorphous phases should be larger than the SLD contrast between the pseudohexagonal and amorphous phases. Depending on this, the variance of the theoretical density contrast upon cooling is illustrated in Figure 3c. If the pseudohexagonal-to-triclinic solid−solid transition occurs at T_B, the density contrast would significantly increase after transformation from pseudohexagonal crystals to α-crystals. Furthermore, the larger density contrast would have a stronger scattering invariant ($Q_{inv} \sim \Delta\rho^2$); thus, Q_{inv} is expected to have a significant increase after the pseudohexagonal-to-triclinic solid−solid transformation. As illustrated in Figure 3c, the experimental Q_{inv} decreases successively in temperature ranges of 250−200 and 110−30 °C, which is consistent with the change in the theoretical density contrast upon cooling because of different thermal expansion coefficients between the crystal and amorphous (*cf.* Supporting Information Density changes due to thermal expansion). However, instead of an abrupt change, a relatively gradual increase of the invariant from 200 to 110 °C is observed; the increase of Q_{inv} below 200 °C corresponds to the formation of the mesomorphic phase, as shown in WAXS analyses in Figure 3a, and Q_{inv} increases rapidly after the α-phase emergence at 150 °C. Based on Figure 3a, the phase composition changes only insignificantly below *ca.* 100 °C and the corresponding Q_{inv} decreases upon cooling, which agrees with the theoretical calculation. Therefore, the simultaneous *in situ* SAXS/WAXS profiles show that the formation of the α-phase in nylon 6/6 is not *via* the route of direct solid−solid transformation, but via the nucleation and growth processes.

The SAXS/WAXS results suggest the existence of the intermediate mesomorphic phase between the high-temperature phase and α-phase. The FITR spectra could further support the mechanism during Brill transition and the subsequent cooling by investigating the behaviors of functional groups. The reduced FTIR spectra of nylon 6/6 upon cooling that were subtracted with the spectrum at 250 °C (pure pseudohexagonal structure region) are illustrated in Figure 4,

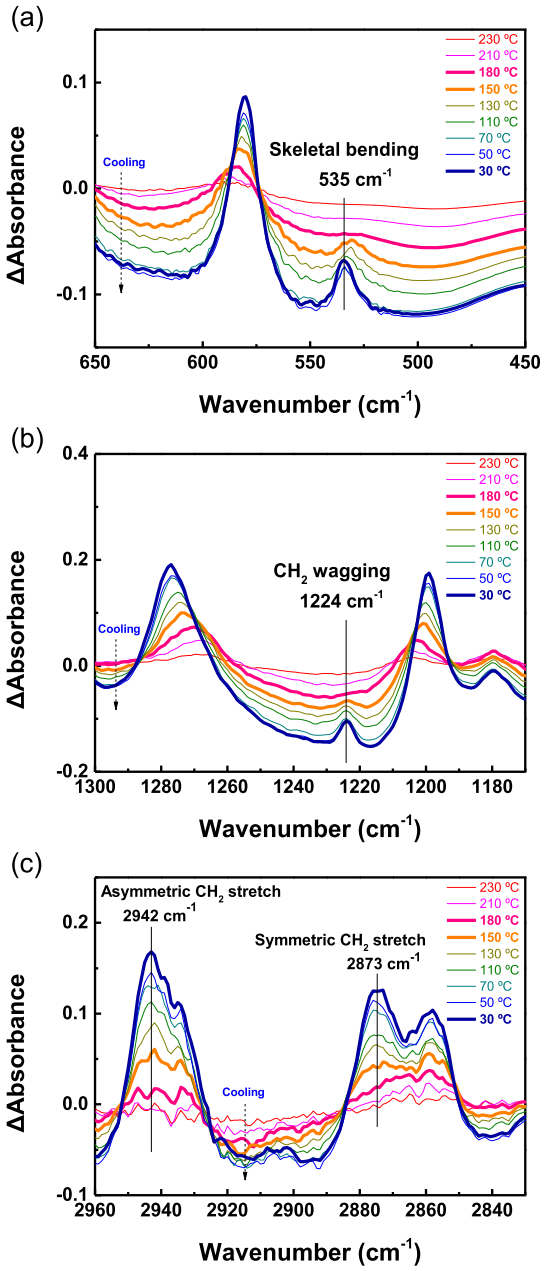

Figure 4. Reduced FTIR cooling spectra based on the 250 °C spectrum of nylon 6/6 at a 10 °C/min rate. The evolutions of methylene linkage vibration including (a) skeletal bending (535 cm^{-1}), (b) CH_2 wagging (1224 cm^{-1}), and (c) symmetric and asymmetric CH_2 stretching (2873 and 2942 cm^{-1}), which show that these absorbance peaks emerge at 150 °C and gradually intensify until 30 °C, implying the appearance of the low-temperature α-phase, which is consistent with the WAXS results. [*cf.* Figure S12 for original FTIR spectra].

revealing that the peaks related to the vibrations of methylene linkage including skeletal bending (535 cm^{-1}), CH_2 wagging (1224 cm^{-1}), and stretching (2873 and 2942 cm^{-1})[11,19−21] appear at 150 °C and the absorbance increases continuously until 30 °C. The emergence of two additional symmetry and asymmetry CH_2 stretching peaks located at a higher wavenumber represents that parts of methylene need more energy

https://dx.doi.org/10.1021/acsapm.0c01303
ACS Appl. Polym. Mater. 2021, 3, 1042−1051

to stretch, suggesting the stiffening of the backbone; furthermore, the skeletal bending and CH_2 wagging imply the order and zigzag chain conformation. Therefore, from the evidence of these IR peaks emerging at 150 °C, the generation of rigid chain conformation is found, suggesting the emergence of the low-temperature α-phase that could be confirmed by the WAXS analyses (*cf.* Figure 3a,b). The consistent results between the WAXS and IR analyses not only suggest that the intermediate mesomorphic phase is required but also indicate that the split of $(100/010/110)_H$ reflection in WAXS profiles from 210 to 180 °C stands for the transformation from the pseudohexagonal structure to the mesomorphic intermediate state. Besides, these reduced IR spectra do not show the characteristic peak of the mesomorphic phase, implying that the structure of mesomorphic phase is similar to the pseudohexagonal structure.

Based on the analyses of cooling SAXS/WAXS profiles and FTIR spectra, results denote that the high-temperature phase transform to the mesomorphic phase and the α-phase emerge below 150 °C upon cooling. Apart from that, the phase evolution in the reverse route, that is, upon heating, was also studied, and the nylon 6/6 sample was heated from 30 to 250 °C after quenched by liquid nitrogen from the molten state at 280 °C. Figure 5a shows the WAXS heating profiles of the melt-quenched nylon 6/6 at a 10 °C/min rate. (*cf.* Figure S5 for the corresponding SAXS profiles) According to the deconvoluted WAXS profile, as shown in Figure S3, the profile already gave a weak intensity of $(100)_\alpha$ and $(010/110)_\alpha$ reflection peaks at 30 °C, indicating that the tiny amount of the α-phase already exists after quenching. Compared with the cooling case, as shown in Figure 1, the $(100)_\alpha$ and $(010/110)_\alpha$ reflections seem to merge into a single peak at a lower temperature. Figure 5b presents the evolution of phase composition upon heating along with the corresponding DSC trace. From 50 to 90 °C, the significant increase of ϕ_{meso} accompanied by an exothermic peak at 62 °C stands for the generation of the mesomorphic phase. The increase of ϕ_{meso} below 90 °C is due to the amorphous to α-phases; besides, the more significant increase of ϕ_{meso} than the decrease of $\phi_{amorphous}$ implies the transformation also from the α-phase to mesomorphic phase. Between 90 and 180 °C, the phase composition stays nearly constant, and the mesomorphic phase transforms to the high-temperature phase along with the merging of mesomorphic reflection peaks in the WAXS pattern at 180 °C. The respective reflection peak positions are illustrated in Figure 5c; compared with the cooling case (dash lines), in which T_B is at *ca.* 210 °C (*cf.* Figure 3b), the T_B for the quenched specimen is at *ca.* 180 °C, about 30 °C lower.

Furthermore, the reflection peak positions between the cooling and the melt-quenched heating process are not entirely identical, especially for the α-structure and the mesomorphic phase. For the α-phase, the positions of $(100)_\alpha$ reflection between heating and cooling processes are nearly the same but different in the $(010/110)_\alpha$ reflection, suggesting that, compared with the interchain distance within the hydrogen-bonded chains, the interspacing of the hydrogen-bonded sheets is much affected by the crystallization condition. In the melt-quenched heating process, the α-phase has larger spacing between hydrogen-bonded sheets because of the fact that the $(010/110)_\alpha$ reflection is at a lower-q position and the respective coherence length is smaller than that in the cooling process (*cf.* Figures S7a and S11a). This difference can also be noticed for the high-temperature pseudohexagonal structure,

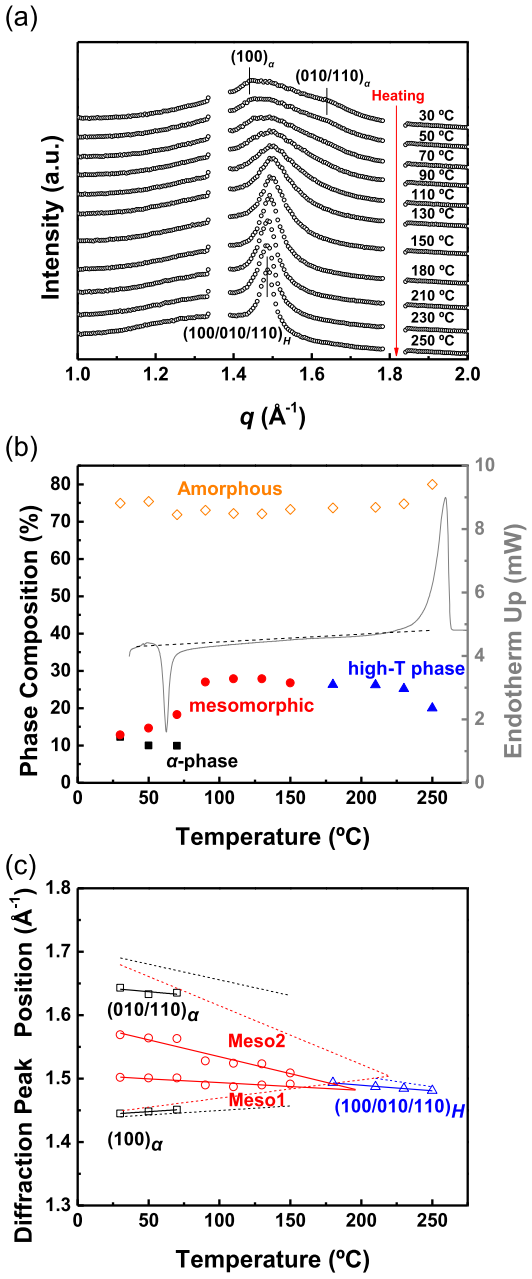

Figure 5. (a) WAXS heating profiles of melt-quenched nylon 6/6 at a 10 °C/min rate. The minor amount of the α-phase can be observed at 30 °C, and the $(100)_\alpha$ and $(010/110)_\alpha$ peaks seem to emerge at a lower temperature than that in the cooling process. (*cf.* Figure 1) (b) Evolution of phase composition (dot symbols) and the corresponding DSC trace (gray line) upon heating, revealing a significant increase of ϕ_{meso} accompanied with an exothermic peak, which represents the generation of the mesomorphic phase and most of the mesomorphic population comes from the α-phase. (c) Evolution of the reflection peak position upon heating. The solid lines are the linear-fit results of the heating process, and the dash lines stand for the linear-fit results of the cooling process, as shown in Figure 3b. Compared with the cooling process, the heating process of the melt-quenched specimen has lower T_B at *ca.* 180 °C.

where the position of $(100/010/110)_H$ reflection in the heating process is at a relatively lower-q position than that in the cooling process, and the high-temperature phase in the heating process give smaller coherence length as well (*cf.* Figures S7a and S11a). These observations imply that the

https://dx.doi.org/10.1021/acsapm.0c01303
ACS Appl. Polym. Mater. 2021, 3, 1042−1051

crystals formed in the heating process are more disordered and loosely packed structures. Besides, the peak evolution of the mesomorphic phase gives a greater discrepancy between the cooling and melt-quenched heating processes, which should be due to different crystallization conditions (*i.e.*, melt-crystallization vs. melt-quenched cold-crystallization). This difference between cooling and heating cases implies that this phase does not have a high degree of order; therefore, this also suggests considering this phase as the mesomorphic phase.

In addition to the peak deconvolution results in WAXS, the IR heating spectra also give supporting observations of the transition from the α-phase to the mesomorphic phase. As shown in Figure 6a, the N−H stretching band reveals a

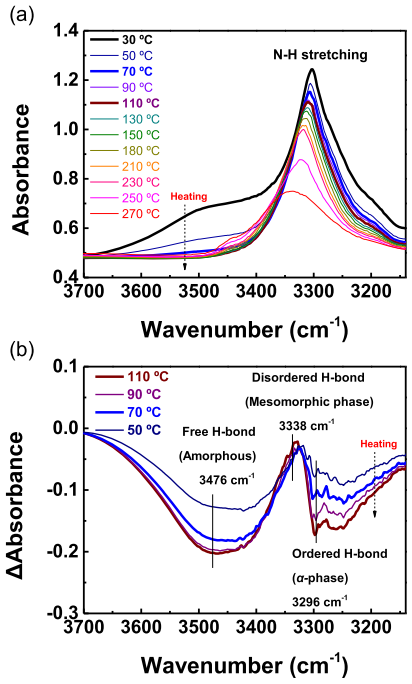

Figure 6. (a) IR spectra of the N−H stretching band showing a significant decrease at a higher wavenumber region from 30 to 110 °C, corresponding to the temperature range of the mesomorphic phase generation in the WAXS profiles. (b) Reduced IR spectra of the N−H stretching band based on the data at 30 °C, revealing that the free and ordered H-bonds decrease, while the disordered H-bond increases, and these changes suggest that the generation of the mesomorphic phase (disordered H-bond) is contributed by the decrease of both the amorphous phase and α-phase (*i.e.*, free and ordered H-bonds).

significant decrease in the higher wavenumber region from 30 to 110 °C, corresponding to the temperature region of the generation of the mesomorphic phase in WAXS profiles. The decrease of the N−H stretching band in higher wavenumber can be interpreted as the decrease of free H-bond, further implying the decline of the amorphous phase; for the same reason, the change in the middle and lowest wavenumber region in the N−H stretching band can be ascribed to disordered and ordered H-bonds, respectively, further implying the change in the mesomorphic and α-phases.[21,57,58] Based on the reduced IR spectra shown in Figure 6b, which subtracted the 30 °C spectrum, the increase of the disordered H-bond (corresponds to the mesomorphic phase) and the decrease of ordered H-bond (α-phase) and free H-bond (amorphous phase) can be noticed from 30 to 110 °C, indicating the increase of the mesomorphic phase accompanied with the decrease of the amorphous phase and α-phase. The IR spectra can be further analyzed by 2D correlation function, and the results are shown in Figure 7. Based on the synchronous

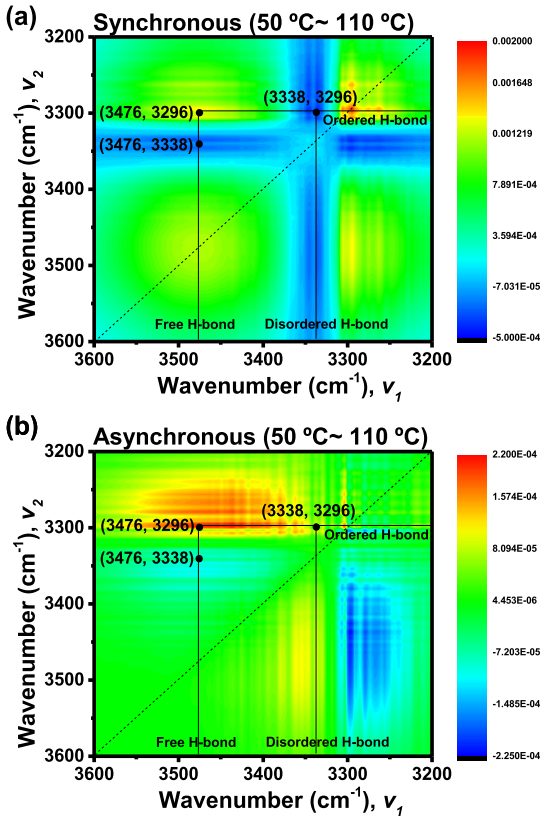

Figure 7. 2D correlation maps of the N−H stretching band in IR spectra. (a) Synchronous and (b) asynchronous patterns showing the increase of the disordered H-bond (mesomorphic phase, 3338 cm^{-1}) predominantly after the decrease of the free H-bond (amorphous phase, 3476 cm^{-1}) and ordered H-bond (α-phase, 3296 cm^{-1}).

pattern (Figure 7a), the disordered H-bond (3338 cm^{-1}) has a negative correlation with both free and ordered H-bonds (3476 and 3296 cm^{-1}), representing that the trend of intensity development upon heating between the disordered H-bond and the free and ordered H-bonds is different; based on the asynchronous pattern, the disordered H-bond has a positive correlation with the ordered H-bond and has a negative correlation with the free H-bond, indicating that the ordered H-bond decreases prior to the increase of the disordered H-bond and the free H-bond decreases prior to the increase of the disordered H-bond. Both the synchronous and asynchronous patterns give a positive correlation between free and ordered H-bonds, denoting that the free H-bond decreases before the decrease of the ordered H-bond. Through the combination of the synchronous and asynchronous patterns, the free H-bond decreases first, followed by the decrease of the ordered H-bond, and finally, the disordered H-bond increases, suggesting that the formation of the mesomorphic phase is due to the amorphous phase and the α-phase, which is consistent with the analyses in WAXS profiles within a 30−110 °C temperature range.

The IR spectra, as shown in Figure 8, are correlated to the α-phase (*cf.* Figure 4), which represents CH_2 wagging and symmetry/asymmetric stretching. At 90 °C, the peak at 1224

https://dx.doi.org/10.1021/acsapm.0c01303
ACS Appl. Polym. Mater. 2021, 3, 1042−1051

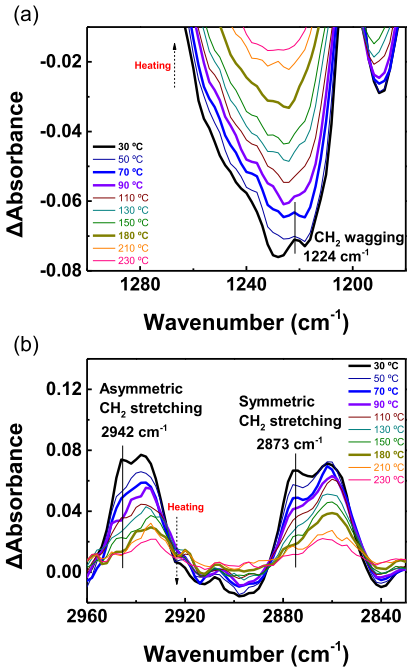

Figure 8. Reduced IR heating spectra of the CH_2 vibration based on the 250 °C spectrum of nylon 6/6. The absorbance of (a) CH_2 wagging disappears and (b) CH_2 symmetric and asymmetric stretching decrease to shoulders at *ca.* 90 °C, indicating the α-phase transformation to the mesomorphic phase. With the subsequent heating, the absorbance of these shoulders successively decreases and vanishes until reaching *ca.* 180 °C, suggesting the structural arrangement from the mesomorphic phase to the high-temperature phase. [*cf.* Figure S13 for original spectra].

cm^{-1} shown in Figure 8a, denoting CH_2 wagging, disappears, and the 2873 and 2942 cm^{-1} peaks shown in Figure 8b, denoting the symmetric and asymmetric CH_2 stretching, also decrease to shoulders, which is consistent with the transition of the α-phase to the mesomorphic phase in WAXS profiles (*cf.* Figure 5b). In the subsequent heating from 90 °C, the absorbance of these two shoulders shown in Figure 8b decreases and vanishes at 180 °C, indicating the transformation from the mesomorphic phase to the high-temperature phase.

CONCLUSIONS

Based on *in situ* SAXS/WAXS, FTIR, and DSC evidences, the existence of the intermediate mesomorphic phase during the Brill transition between the high-temperature pseudohexagonal structure and low-temperature triclinic structure (α-phase) in polyamide 6/6 (nylon 6/6) is confirmed. The significant difference in packing density between the two crystalline forms forbids the direct solid-to-solid transformation path that was suggested previously. In the cooling process, the IR spectra indicate that the α-phase emerges below 150 °C; two additional reflection peaks are required in the deconvoluted WAXS profiles to adequately describe the population changes between T_B (210 °C) and 150 °C, pointing out the existence of the intermediate mesomorphic phase and suggesting that the transition from the high-temperature phase to α-phase involves an intermediate mesomorphic phase. In the heating process of the melt-quenched specimen, tiny amounts of α- and mesomorphic phases already exist at 30 °C. The WAXS profiles and IR spectra denote that the α-phase melt completely at 90 °C and, in the meantime, the population of the mesomorphic phase increases; the mesomorphic phase finally transforms to the pseudohexagonal structure at 180 °C. As both cooling and heating processes demonstrate the existence of the intermediate mesomorphic phase (instead of the previously believed solid−solid pseudohexagonal-to-triclinic process), Brill transition involves a progressive transformation among the high-temperature phase, mesomorphic phase, and α-phase. According to the comprehensive understanding of the Brill transition in nylon 6/6, one would expect significant time dependence of morphology and mechanical properties in the vicinity of the Brill transition, especially upon transient exposure.

ASSOCIATED CONTENT

Supporting Information

The Supporting Information is available free of charge at https://pubs.acs.org/doi/10.1021/acsapm.0c01303.

Schematic WAXS deconvoluted profiles; SAXS profiles; conformational change during phase transformation; original FTIR spectra; and density changes due to thermal expansion (PDF)

AUTHOR INFORMATION

Corresponding Authors

Po-Hsun Chen − *Department of Chemical Engineering, National Tsing Hua University, Hsinchu 30013, Taiwan;* orcid.org/0000-0002-3670-8241; Email: zero00023@gapp.nthu.edu.tw

An-Chung Su − *Department of Chemical Engineering, National Tsing Hua University, Hsinchu 30013, Taiwan;* Email: acsu@mx.nthu.edu.tw

Authors

Cheng-Yo Ho − *Department of Chemical Engineering, National Tsing Hua University, Hsinchu 30013, Taiwan*

Ching-Feng Yang − *Department of Chemical Engineering, National Tsing Hua University, Hsinchu 30013, Taiwan*

U-Ser Jeng − *Department of Chemical Engineering, National Tsing Hua University, Hsinchu 30013, Taiwan; National Synchrotron Radiation Research Center, Hsinchu 30076, Taiwan;* orcid.org/0000-0002-2247-5061

Complete contact information is available at: https://pubs.acs.org/10.1021/acsapm.0c01303

Notes

The authors declare no competing financial interest.

ACKNOWLEDGMENTS

Financial support from the Ministry of Science and Technology (MoST 101-2221-E-007-037-MY3) is gratefully acknowledged. The team members of TLS BL23A and NSRRC are thanked for beamline alignment and technical support.

REFERENCES

(1) Gilbert, M. Aliphatic polyamides. In *Brydson's Plastics Materials*; Elsevier, 2017; pp 487−511.

(2) Brill, R. über das Verhalten von Polyamiden beim Erhitzen. *J. Prakt. Chem.* **1942**, *161*, 49−64.

(3) Colclough, M. L.; Baker, R. Polymorphism in Nylon 66. *J. Mater. Sci.* **1978**, *13*, 2531−2540.

(4) Ramesh, C.; Keller, A.; Eltink, S. J. E. A. Studies on the Crystallization and Melting of Nylon-6, 6: 1. The Dependence of the Brill Transition on the Crystallization Temperature. *Polymer* **1994**, *35*, 2483−2487.
(5) Xenopoulos, A.; Wunderlich, B. Conformational Motion and Disorder in Aliphatic Nylons the Case of Nylon 6.6. *Colloid Polym. Sci.* **1991**, *269*, 375−391.
(6) Feldman, A. Y.; Wachtel, E.; Vaughan, G. B. M.; Weinberg, A.; Marom, G. The brill transition in transcrystalline nylon-66. *Macromolecules* **2006**, *39*, 4455−4459.
(7) Wolanov, Y.; Feldman, A. Y.; Harel, H.; Marom, G. Amorphous and crystalline phase interaction during the Brill transition in nylon 66. *Express Polym. Lett.* **2009**, *3*, 452−457.
(8) Yoshioka, Y.; Tashiro, K. Structural Change in the Brill Transition of Nylon m/n (1) Nylon 10/10 and Its Model Compounds. *Polymer* **2003**, *44*, 7007−7019.
(9) Itoh, T. Change with Temperature in Crystal Structures of Nylons 6, 66 and 610. *Jpn. J. Appl. Phys.* **1976**, *15*, 2295−2306.
(10) Murthy, N. S.; Curran, S. A.; Aharoni, S. M.; Minor, H. Premelting Crystalline Relaxations and Phase Transitions in Nylon 6 and 6, 6. *Macromolecules* **1991**, *24*, 3215−3220.
(11) Cooper, S. J.; Coogan, M.; Everall, N.; Priestnall, I. A Polarised μ-FTIR Study on a Model System for Nylon 6 6: Implications for the Nylon Brill Structure. *Polymer* **2001**, *42*, 10119−10132.
(12) Hirschinger, J.; Miura, H.; Gardner, K. H.; English, A. D. Segmental Dynamics in the Crystalline Phase of Nylon 66: Solid State Deuterium NMR. *Macromolecules* **1990**, *23*, 2153−2169.
(13) Vasanthan, N.; Murthy, N. S.; Bray, R. G. Investigation of Brill Transition in Nylon 6 and Nylon 6, 6 by Infrared Spectroscopy. *Macromolecules* **1998**, *31*, 8433−8435.
(14) Starkweather, H. W., Jr.; Jones, G. A. Crystalline transitions in powders of nylon 66 crystallized from solution. *J. Polym. Sci., Polym. Phys. Ed.* **1981**, *19*, 467−477.
(15) Menezes, D. B.; Reyer, A.; Musso, M. Investigation of the Brill transition in nylon 6, 6 by Raman, THz-Raman, and two-dimensional correlation spectroscopy. *Spectrochim. Acta, Part A* **2018**, *190*, 433−441.
(16) Wendoloski, J. J.; Gardner, K. H.; Hirschinger, J.; Miura, H.; English, A. D. Molecular dynamics in ordered structures: computer simulation and experimental results for nylon 66 crystals. *Science* **1990**, *247*, 431−436.
(17) Yoshioka, Y.; Tashiro, K.; Ramesh, C. Structural Change in the Brill Transition of Nylon m/n (2) Conformational Disordering as Viewed from the Temperature-Dependent Infrared Spectral Measurements. *Polymer* **2003**, *44*, 6407−6417.
(18) Vasanthan, N. Crystallinity determination of nylon 66 by density measurement and fourier transform infrared (FTIR) spectroscopy. *J. Chem. Educ.* **2012**, *89*, 387−390.
(19) Jakeš, J.; Krimm, S. A valence force field for the amide group. *Spectrochim. Acta, Part A* **1971**, *27*, 19−34.
(20) Charles, J.; Ramkumaar, G.; Azhagiri, S.; Gunasekaran, S. FTIR and thermal studies on nylon-66 and 30% glass fibre reinforced nylon-66. *J. Chem.* **2009**, *6*, 23−33.
(21) Luo, J.; Zhou, T.; Fu, X.; Liang, H.; Zhang, A. Mechanism in Brill Transition of Polyamide 66 Studied by Two-Dimensional Correlation Infrared Spectroscopy. *Eur. Polym. J.* **2011**, *47*, 230−237.
(22) Menezes, D. B.; Reyer, A.; Musso, M. Analysis of the Brill transition and reversible brill transition in nylon 6, 6 by Raman spectroscopy. *Spectroscopy* **2016**, *31*, 44−48.
(23) Pepin, J.; Miri, V.; Lefebvre, J.-M. New Insights into the Brill Transition in Polyamide 11 and Polyamide 6. *Macromolecules* **2016**, *49*, 564−573.
(24) Ramesh, C.; Gowd, E. B. High-temperature X-ray Diffraction Studies on the Crystalline Transitions in the α-and γ-forms of Nylon-6. *Macromolecules* **2001**, *34*, 3308−3313.
(25) Auriemma, F.; Petraccone, V.; Parravicini, L.; Corradini, P. Mesomorphic form (β) of nylon 6. *Macromolecules* **1997**, *30*, 7554−7559.
(26) Radusch, H.-J.; Stolp, M.; Androsch, R. Structure and Temperature-induced Structural Changes of Various Polyamides. *Polymer* **1994**, *35*, 3568−3571.
(27) Kim, K. G.; Newman, B. A.; Scheinbeim, J. I. Temperature dependence of the crystal structures of nylon 11. *J. Polym. Sci., Polym. Phys. Ed.* **1985**, *23*, 2477−2482.
(28) Tashiro, K. Structural phase transition of aliphatic nylons viewed from the WAXD/SAXS and vibrational spectral measurements and molecular dynamics calculation. *Chin. J. Polym. Sci.* **2007**, *25*, 73−82.
(29) Li, W.; Huang, Y.; Zhang, G.; Yan, D. Investigation on Brill transition of nylons 6/16, 4/16 and 2/16 by variable-temperature WAXD and FTIR. *Polym. Int.* **2003**, *52*, 1905−1908.
(30) Zhang, G.; Watanabe, T.; Yoshida, H.; Kawai, T. Phase Transition Behavior of Nylon-66, Nylon-48, and Blends. *Polym. J.* **2003**, *35*, 173−177.
(31) Jones, N. A.; Atkins, E. D. T.; Hill, M. J.; Cooper, S. J.; Franco, L. Chain-folded lamellar crystals of aliphatic polyamides. Comparisons between nylons 4 4, 6 4, 8 4, 10 4, and 12 4. *Macromolecules* **1996**, *29*, 6011−6018.
(32) Jones, N. A.; Atkins, E. D. T.; Hill, M. J.; Cooper, S. J.; Franco, L. Polyamides with a Choice of Structure and Crystal Surface Chemistry. Studies of Chain-Folded Lamellae of Nylons 8 10 and 10 12 and Comparison with the Other 2 N 2 (N+ 1) Nylons 4 6 and 6 8. *Macromolecules* **1997**, *30*, 3569−3578.
(33) Jones, N. A.; Atkins, E. D. T.; Hill, M. J.; Cooper, S. J.; Franco, L. Chain-folded lamellar crystals of aliphatic polyamides. Investigation of nylons 4 8, 4 10, 4 12, 6 10, 6 12, 6 18 and 8 12. *Polymer* **1997**, *38*, 2689−2699.
(34) Jones, N. A.; Atkins, E. D. T.; Hill, M. J. Investigation of solution-grown, chain-folded lamellar crystals of the even-even nylons: 6 6, 8 6, 8 8, 10 6, 10 8, 10 10, 12 6, 12 8, 12 10, and 12 12. *J. Polym. Sci., Part A: Polym. Chem.* **2000**, *38*, 1209−1221.
(35) Jones, N. A.; Atkins, E. D. T.; Hill, M. J. Comparison of structures and behavior on heating of solution-grown, chain-folded lamellar crystals of 31 even− even nylons. *Macromolecules* **2000**, *33*, 2642−2650.
(36) Morales-Gámez, L.; Soto, D.; Franco, L.; Puiggalí, J. Brill Transition and Melt Crystallization of Nylon 56: An Odd-Even Polyamide with Two Hydrogen-Bonding Directions. *Polymer* **2010**, *51*, 5788−5798.
(37) Morales-Gámez, L.; Casas, M. T.; Franco, L.; Puiggalí, J. Structural Transitions of Nylon 47 and Clay Influence on Its Crystallization Behavior. *Eur. Polym. J.* **2013**, *49*, 1354−1364.
(38) Yang, X.; Tan, S.; Li, G.; Zhou, E. Dependence of the Brill Transition on the Crystal Size of Nylon 10 10. *Macromolecules* **2001**, *34*, 5936−5942.
(39) Yan, D.; Li, Y.; Zhu, X. Brill Transition in Nylon 10 12 Investigated by Variable Temperature XRD and Real Time FT-IR. *Macromol. Rapid Commun.* **2000**, *21*, 1040−1043.
(40) Vinken, E.; Terry, A. E.; Hoffmann, S.; Vanhaecht, B.; Koning, C. E.; Rastogi, S. Influence of hydrogen bonding on the conformational changes, the brill transition, and lamellae thickening in (co) polyamides. *Macromolecules* **2006**, *39*, 2546−2552.
(41) Hill, M. J.; Atkins, E. D. T. Morphology and structure of nylon 68 single crystals. *Macromolecules* **1995**, *28*, 604−609.
(42) Cavallo, D.; Gardella, L.; Alfonso, G. C.; Portale, G.; Balzano, L.; Androsch, R. Effect of cooling rate on the crystal/mesophase polymorphism of polyamide 6. *Colloid Polym. Sci.* **2011**, *289*, 1073−1079.
(43) Mileva, D.; Androsch, R.; Zhuravlev, E.; Schick, C. Morphology of mesophase and crystals of polyamide 6 prepared in a fast scanning chip calorimeter. *Polymer* **2012**, *53*, 3994−4001.
(44) Strobl, G. From the melt via mesomorphic and granular crystalline layers to lamellar crystallites: A major route followed in polymer crystallization? *Eur. J. Phys. Educ.* **2000**, *3*, 165−183.
(45) Yang, C.-F.; Huang, Y.-F.; Ruan, J.; Su, A.-C. Extensive Development of Precursory Helical Pairs Prior to Formation of

https://dx.doi.org/10.1021/acsapm.0c01303
ACS Appl. Polym. Mater. 2021, 3, 1042−1051

Stereocomplex Crystals in Racemic Polylactide Melt Mixture. *Macromolecules* **2012**, *45*, 872−878.
(46) Lan, Y.-K.; Su, A.-C. Primary nucleation of polyethylene: Embryogenesis from a semidilute solution. *Polymer* **2014**, *55*, 3087−3092.
(47) Cheng, S. Z. D. Chapter 2-Thermodynamics and Kinetics of Phase Transitions. In *Phase Transitions in Polymers*; Cheng, S. Z. D., Ed.; Elsevier: Amsterdam, 2008; pp 17-59.
(48) Chen, S. H.; Su, A. C.; Su, C. H.; Chen, S. A. Phase Behavior of Poly(9, 9-di-n-hexyl-2, 7-fluorene). *J. Phys. Chem. B* **2006**, *110*, 4007−4013.
(49) Gan, Z.; Kuwabara, K.; Abe, H.; Iwata, T.; Doi, Y. Metastability and transformation of polymorphic crystals in biodegradable poly (butylene adipate). *Biomacromolecules* **2004**, *5*, 371−378.
(50) Jeng, U.-S.; Su, C. H.; Su, C.-J.; Liao, K.-F.; Chuang, W.-T.; Lai, Y.-H.; Chang, J.-W.; Chen, Y.-J.; Huang, Y.-S.; Lee, M.-T.; Yu, K.-L.; Lin, J.-M.; Liu, D.-G.; Chang, C.-F.; Liu, C.-Y.; Chang, C.-H.; Liang, K. S. A Small/Wide-Angle X-Ray Scattering Instrument for Structural Characterization of Air−Liquid Interfaces, Thin Films and Bulk Specimens. *J. Appl. Crystallogr.* **2010**, *43*, 110−121.
(51) Chen, S.-H.; Lin, T.-L. Chapter 16. Colloidal Solutions. In *Methods in Experimental Physics*; Price, D. L., Sköld, K., Eds.; Academic Press, 1987; Vol. *23*, pp 489−543.
(52) Chuang, W.-T.; Jeng, U.-S.; Sheu, H.-S.; Hong, P.-D. Competition between Phase Separation and Crystallization in a PCL/PEG Polymer Blend Captured by Synchronized SAXS, WAXS, and DSC. *Macromol. Res.* **2006**, *14*, 45−51.
(53) Feigin, L.; Svergun, D. I. *Structure Analysis by Small-Angle X-Ray and Neutron Scattering*; Plenum: New York, 1987; Vol. *1*, pp 59−105.
(54) Noda, I.; Dowrey, A. E.; Marcott, C. Two-Dimensional Infrared (2D IR) Spectroscopy. A New Tool for Interpreting Infrared Spectra. *Microchim. Acta* **1988**, *94*, 101−103.
(55) Noda, I. Two-Dimensional Infrared Spectroscopy. *J. Am. Chem. Soc.* **1989**, *111*, 8116−8118.
(56) Noda, I.; Dowrey, A. E.; Marcott, C. Recent Developments in Two-Dimensional Infrared (2D IR) Correlation Spectroscopy. *Appl. Spectrosc.* **1993**, *47*, 1317−1323.
(57) Skrovanek, D. J.; Painter, P. C.; Coleman, M. M. Hydrogen Bonding in Polymers. 2. Infrared Temperature Studies of Nylon 11. *Macromolecules* **1986**, *19*, 699−705.
(58) Coleman, M. M.; Lee, K. H.; Skrovanek, D. J.; Painter, P. C. Hydrogen Bonding in Polymers. 4. Infrared Temperature Studies of a Simple Polyurethane. *Macromolecules* **1986**, *19*, 2149−2157.

https://dx.doi.org/10.1021/acsapm.0c01303
ACS Appl. Polym. Mater. 2021, 3, 1042−1051